Available online at www.sciencedirect.com

SciVerse ScienceDirect

Journal of the European Ceramic Society 32 (2012) 1251–1259

www.elsevier.com/locate/jeurceramsoc

Structural evolution, sintering behavior and microwave dielectric properties of $(1-x)Li_3NbO_4$–$xLiF$ $(0 \leq x \leq 0.9)$

J.J. Bian *, J.Y. Wu, L. Wang

Department of Inorganic Materials, Shanghai University, 149 Yanchang Road, Shanghai 200072, China

Received 3 November 2011; received in revised form 13 December 2011; accepted 14 December 2011
Available online 11 January 2012

Abstract

Sintering behavior, microstructure and microwave dielectric properties of $(1-x)Li_3NbO_4$–$xLiF$ $(0 \leq x \leq 0.9)$ ceramics have been studied in this paper. Continuous solid solution with rock salt structure formed across the entire compositional range. Phase transformed from ordered body-centered cubic phase to short range ordered face-centered cubic phase with the addition of LiF. The $x > 0.4$ compositions could be densified at 850 °C/2 h. The optimized $Q \times f$ value for each composition increased with the increase of LiF content and saturated at about 75,000 GHz when $x \geq 0.15$, whereas the optimized dielectric permittivity decreased with the increase of LiF content. All specimens exhibited negative τ_f value. The chemical compatibilities with copper (Cu) in the case of $x = 0.4$ composition and silver (Ag) in the case of $x = 0.5$ composition were also investigated, respectively. No chemical reaction has taken place between the matrix phase and Ag or Cu after sintering at 850 °C/2 h or 950 °C/2 h, respectively.
© 2012 Elsevier Ltd. All rights reserved.

Keywords: LTCC; Dielectric properties

1. Introduction

Low-temperature co-fired ceramics (LTCCs) with suitable dielectric properties have been widely investigated.[1–6] Reducing the sintering temperature without affecting the properties is a challenging problem in LTCC material research. Glass-free LTCC material with appropriate microwave dielectric properties is strongly desired for the multilayer structure applications. Since addition of low melting glass either leads to poor microwave dielectric properties or significantly increases the possibility of chemical interaction with the metal electrode due to the presence of complicated phases in the LTCC system.[7–9] Recently a number of glass-free LTCC microwave dielectrics have been reported.[10–20] However, many problems existed, such as chemical incompatibility with Ag/Cu electrodes and/or large τ_f values, which prevent their LTCC applications. Furthermore, some compounds have a sintering temperature lower than 700 °C, which is not compatible with the sintering of Ag or Cu. Above all, most of the compounds reported exhibit very narrow window for tuning the sintering temperature and microwave dielectric properties, in particular the τ_f value, due to their fixed compositions. Therefore the search for an ideal glass-free low-temperature fired material with good properties is still continuing. Up to now, the search for the composition of glass-free LTCC is mostly by try and error method based on the phase diagram. In general constituent with low-melting point, such as Bi_2O_3, TeO_2, P_2O_5, V_2O_5, is included. Crystal chemistry is helpful in designing glass-free LTCC materials. Recently we proposed the designing guidelines for glass-free LTCC materials from the point view of crystal chemistry.[21] Both the bond nature (bond strength and polarity) and atomic packing fraction play important roles in controlling the sintering temperature and microwave dielectric properties. The less the packing fraction or bond strength, the lower the sintering temperature. Thus we can tune the sintering temperature and structure dependent microwave dielectric properties in wide range by controlling the lattice packing fraction, bond strength and polarity through forming solid solution. As an example, we have successfully designed several glass-free LTCC materials by crystal chemistry.[21,22]

For most of the compounds with sintering temperature lower than 950 °C, generally low packing fraction for the

* Corresponding author.
E-mail address: jjbian@shu.edu.cn (J.J. Bian).

0955-2219/$ – see front matter © 2012 Elsevier Ltd. All rights reserved.
doi:10.1016/j.jeurceramsoc.2011.12.026

lattice (<60%) and/or weak oxygen bond existed.[21] In search for new materials with low sintering temperature, therefore, we usually look to open and/or weak bonded crystal structure in which rapid mass diffusions can occur. Li_3NbO_4 with ternary rock salt type structure exhibits relatively low sintering temperature due to their weak oxygen bond valence sum (BVS(O) = 1.884) irrespective of their little high packing fractions (68%). It also shows good microwave dielectric properties: $\varepsilon_r = 16.4$, $\tau_f = -45$ ppm/°C and $Q \times f = 47{,}179$ GHz (8.7 GHz) when sintered at 1150 °C/2 h.[23] D. Zhou et al.[24] reported that Li_3NbO_4 could be well sintered around 930 °C (97% theoretical density), and was found not to react with Ag at 900 °C. The best microwave dielectric properties were obtained in the ceramic sintered at 930 °C for 2 h with permittivity 15.8, $Q \times f$ value about 55,009 GHz, and temperature coefficient about −49 ppm/°C.[24] The difference in sintering temperature may be related to the different synthesizing conditions of Li_3NbO_4. In our previous study, Li_3NbO_4 was synthesized at 900 °C for 2 h, whereas 800 °C/2 h was adopted in the report of D. Zhou et al. Anyway, the sintering temperature of pure Li_3NbO_4 is still little higher for the co-firing with Ag. The sintering temperature should be further reduced to 850 °C in order to co-fire with pure Ag electrode.

Li_3NbO_4 is a ternary rock salt type oxide in which Pauling's rule of electrovalence is not satisfied because the cation ratio does not permit electroneutrality around any oxygen. The space group of Li_3NbO_4 was first reported to be I23,[25] and later revised to be I-43m.[26] The most striking feature of Li_3NbO_4 is the presence of Nb_4O_{16} clusters which form a body-centered cubic lattice with Li ions located among the Nb_4O_{16} clusters. Ordering distribution of clusters of edge-sharing NbO6 octahedra and LiO6 octahedra are responsible for the superstructure.[27] LiF has the face centered cubic rock salt structure. Continuous solid solutions between Li_3NbO_4 and LiF are expected to form due to their similar rock salt type crystal structure (edge-sharing of cation oxygen octahedra) and ionic size. The oxygen bond strength should decrease with the increasing substitution of F^- for O^{2-}. Hence, the sintering temperature of the solid solution is also expected to decrease with the increase of LiF addition according to the aforementioned guideline.

In this paper, we studied the effect of LiF addition on the structural evolution, sintering behavior and microwave dielectric properties of $(1-x)Li_3NbO_4$–xLiF ceramics. The sintering behavior of Li_3NbO_4 was also reinvestigated in this paper.

2. Experimental

$(1-x)Li_3NbO_4$–xLiF ($0 \le x \le 0.9$) powders were prepared by two-steps process. First Li_3NbO_4 was synthesized at 900 °C/2 h by conventional solid-state reaction process from the starting materials including Nb_2O_5 (99.9%), Li_2CO_3 (99.9%) (first method). For the purpose of binding of lithium component, the initial mixtures were subjected to preliminary low-temperature calcining at 500 °C for 20 h and subsequent calcining at 900 °C for 2 h (second method). Then the synthesized Li_3NbO_4 by second method was added with different amount of LiF (99.8%) according to the above formula, and then mixed with ZrO_2 balls in ethanol for 24 h. The slurry was dried and well ground. After drying, mixed with 7 wt% PVA and sieving, the granulated powders were uniaxially pressed into pellets 10 mm in diameter and 4.5 mm in thickness under a pressure of 120 MPa. The pellets were sintered at the temperatures ranging from 850 °C to 1150 °C for 2 h. The sintering temperature decreased with the increase of LiF content, and was optimized by the maximum bulk density and $Q \times f$ value. In order to prevent lithium evaporation and possible pyrohydrolysis or oxidation of F^- during the sintering, the compacts were covered with sacrificial powder of the same composition and sintered in the dry N_2 atmosphere. The chemical compatibility with silver or copper was investigated by co-firing the mixed powders with pure silver (30 wt% Ag) or copper (30 wt% Cu) in ambient atmosphere at temperature of 850 °C for 2 h or N_2 atmosphere at 950 °C for 2 h, respectively.

The densities of the ceramics were measured by the Archimedes method. The phase compositions of the sintered specimens were identified by X-ray powder diffraction (XRD) with Ni-filtered Cu Kα radiation (Rigaku D\max2550, Tokyo, Japan). The unit cell parameters were refined by a least-squares procedure via Jade 5.0 software. The Raman experiments were carried out for the sintered samples (RENIShaw in Via plus, UK). The Raman spectra were excited with the 785 nm line of a semiconductor laser at a power of 250 mW and recorded in backscattering geometry using InVia Raman Microscope equipped with a grating filter, enabling good stray light rejection in the 100–1000 cm range. The microstructures of the sintered samples were characterized by scanning electron microscopy (SEM, Model JSM-6700F, JEOL, Tokyo, Japan). Some of the samples were selected to be polished and thermally etched at the temperature of 100 °C lower than its sintering temperature for 30 min. Chemical compositions were analyzed by energy dispersive spectrometer (EDS) (INCA EDS, Oxford, UK). Microwave dielectric properties of the sintered specimens were measured at about 9–13 GHz using a network analyzer (Model N5230A, Agilent, Palo Alto, CA). The quality factor was measured by the transmission cavity method. The relative dielectric constant (ε_r) was measured according to the Hakki–Coleman method with the TE_{011} resonant mode, and the temperature coefficient of the resonator frequency (τ_f) was measured using invar cavity in the temperature range from 20 to 80 °C.

3. Results and discussions

Fig. 1 shows the XRD powder patterns of $(1-x)Li_3NbO_4$–xLiF ($0 \le x \le 0.9$) sintered at different temperatures. It can be seen that all samples exhibited single phase and continuous solid solution formed across the entire compositional range. The $x \le 0.5$ compositions exhibited the same ordered body-centered cubic phase as that of pure Li_3NbO_4, whereas, the $x > 0.5$ compositions exhibited the same face-centered cubic (S.G.: Fm-3m) rock salt structure as LiF (Fig. 1A). It implies a long-range disordering distribution of cations for the $x > 0.5$ compositions. Furthermore phase transition from ordered body-centered cubic phase to disordered

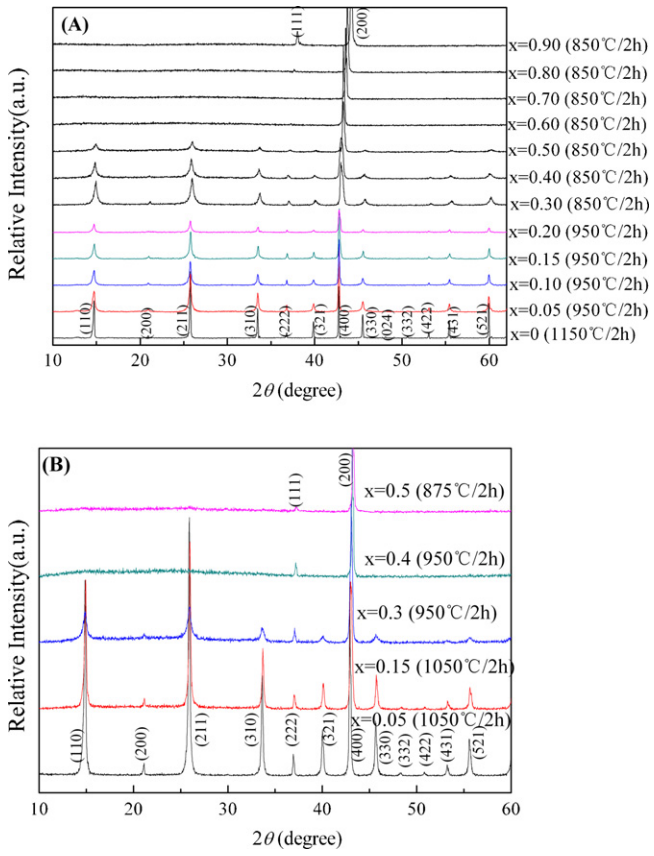

Fig. 1. XRD powder patterns of $(1-x)Li_3NbO_4$–$xLiF$ ($0<x\leq 0.9$) sintered at different temperatures.

face-centered cubic phase also occurred for $x=0.4$ and $x=0.5$ compositions when their sintering temperature increased from 850 °C/2 h to 950 and 875 °C/2 h, respectively (Fig. 1B). Considering the possibility of phase transformation caused by the Li- and F-loss during the heat treatment at the higher temperature, the weight losses of $x\geq 0.3$ compositions after sintering at different conditions are illustrated in Fig. 2. The weight loss of the sintered specimen (muffled with sacrificial powder of the same composition) is less than 1 wt%, whereas the weight loss of the unmuffled specimen ($x=0.5$) sintered

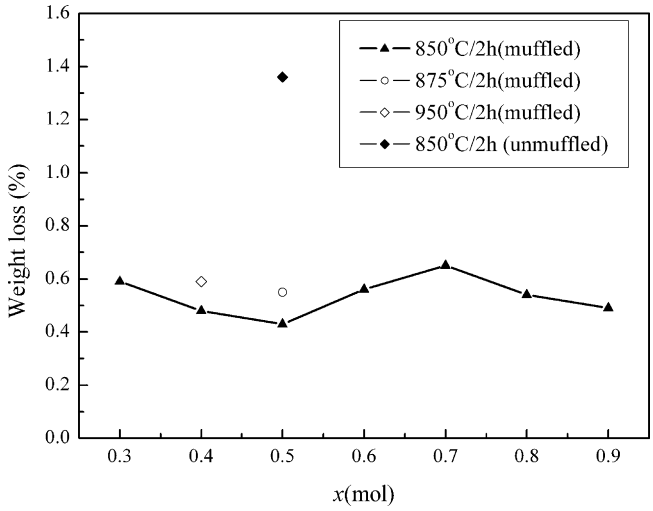

Fig. 2. Variation of weight loss after sintering at different conditions as function of x.

850 °C/2 h is about 1.36 wt%. The Li- and F-evaporation could be substantially suppressed by being muffled with sacrificial powder of the same composition. It indicates that the order–disorder phase transition temperature decreased with increasing LiF content. Similar phenomenon is also observed in the case of Li_2TiO_3–MgO system, in which the order–disorder phase transition temperature decreases with the increase of MgO addition.[28] Change of the lattice constant as function of LiF content is shown in Table 1. The lattice constant decreased with the increase of LiF content as expected. Variation of the cell volume can be clarified by considering their relative ionic sizes ($R_{Li^+}=0.76$ Å, $R_{Nb^{5+}}=0.64$ Å, $R_{O^{2-}}=1.40$ Å, $R_{F^-}=1.33$ Å).[29] The general formula of the composition is $Li_{(12-8x/4-3x)}Nb_{(4-4x/4-3x)}O_{(16-16x/4-3x)}F_{(4x/4-3x)}$ (normalized to Li_3NbO_4 type) when $x<0.4$ and $Li_{(3-2x/4-3x)}Nb_{(1-x/4-3x)}O_{(4-4x/4-3x)}F_{(x/4-3x)}$ (normalized to LiF type) when $x\geq 0.4$, respectively. Variation of comparative ionic size with substituting content for each AB type rock salt molecule is $(-0.4x/4-3x)$. The ionic size and thus the cell volume are expected to decrease with increasing x.

Table 1
Variation of lattice parameters of $(1-x)Li_3NbO_4$–$xLiF$ ($0\leq x\leq 0.9$) with x. (For comparison, the data of $x=1.0$ composition, which was from ICSD #62361, was also appended here.) S.T., sintering temperature; TD, theoretical density.

Composition	Formula	S.T. (°C)	S.G.	a (Å)	Z	TD (g/cm^3)
$x=0.0$	Li_3NbO_4		I-43m	8.4282(2)	8	3.94
$x=0.05$	$Li_{3.013}Nb_{0.987}O_{3.948}F_{0.052}$	1050	I-43m	8.4251(4)	8	3.93
$x=0.1$	$Li_{3.027}Nb_{0.973}O_{3.892}F_{0.108}$	1050	I-43m	8.4187(6)	8	3.91
$x=0.15$	$Li_{3.042}Nb_{0.958}O_{3.831}F_{0.169}$	1050	I-43m	8.4147(15)	8	3.89
$x=0.2$	$Li_{3.059}Nb_{0.941}O_{3.765}F_{0.235}$	1050	I-43m	8.4094(10)	8	3.87
$x=0.3$	$Li_{3.097}Nb_{0.903}O_{3.613}F_{0.387}$	950	I-43m	8.3931(14)	8	3.83
$x=0.4$	$Li_{0.7857}Nb_{0.2143}O_{0.8571}F_{0.1429}$	950	Fm-3m	4.1902(8)	4	3.77
$x=0.5$	$Li_{0.8}Nb_{0.2}O_{0.8}F_{0.2}$	875	Fm-3m	4.1848(5)	4	3.70
$x=0.6$	$Li_{0.8182}Nb_{0.1818}O_{0.7273}F_{0.2727}$	850	Fm-3m	4.1763(1)	4	3.59
$x=0.7$	$Li_{0.8421}Nb_{0.1579}O_{0.6316}F_{0.3684}$	850	Fm-3m	4.1550(9)	4	3.48
$x=0.8$	$Li_{0.8750}Nb_{0.1250}O_{0.5}F_{0.5}$	850	Fm-3m	4.1369(2)	4	3.30
$x=0.9$	$Li_{0.9230}Nb_{0.0770}O_{0.3077}F_{0.6923}$	850	Fm-3m	4.0984(6)	4	3.05
$x=1.0$	LiF		Fm-3m	4.027	4	2.64

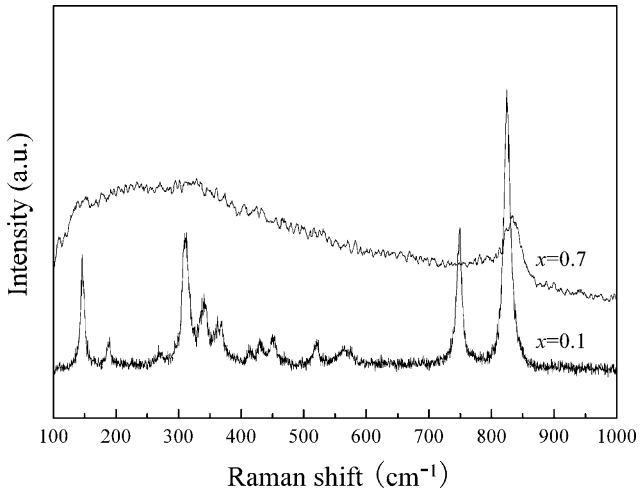

Fig. 3. Raman spectra of $x = 0.1$ and $x = 0.7$ compositions.

Fig. 3 shows the Raman spectra of $x = 0.1$ and $x = 0.7$ compositions, which are typical for the ordered and disordered phase in the XRD patterns (Fig. 1), respectively. The spectrum of $x = 0.1$ is very similar to that of Li_3NbO_4.[23] No first order Raman active mode is expected for the $x = 0.7$ composition, which exhibited completely disordered cubic phase (Fm-3m) as shown in Fig. 1, according to group analysis. However weak broad band at 830 cm^{-1} could be still observed for $x = 0.7$ composition, which excluded the completely random distribution of ions in $x = 0.7$ composition. It indicated that short range ordering (SRO) should exist in the $x = 0.7$ composition, which is in agreement with the observation in Li_3NbO_4–MgO.[23]

Fig. 4 shows variation of relative density with x and sintering temperature. The theoretical density of each composition was calculated from the refined XRD data via Jade 5.0 software (Table 1). The addition of LiF enhanced the sinterability of Li_3NbO_4, and the sintering temperature decreased with the increase of LiF content as expected. The sintering temperature could be reduced to 850 °C/2 h when $x \geq 0.3$. It is confirmed that sintering rates are higher near the order–disorder

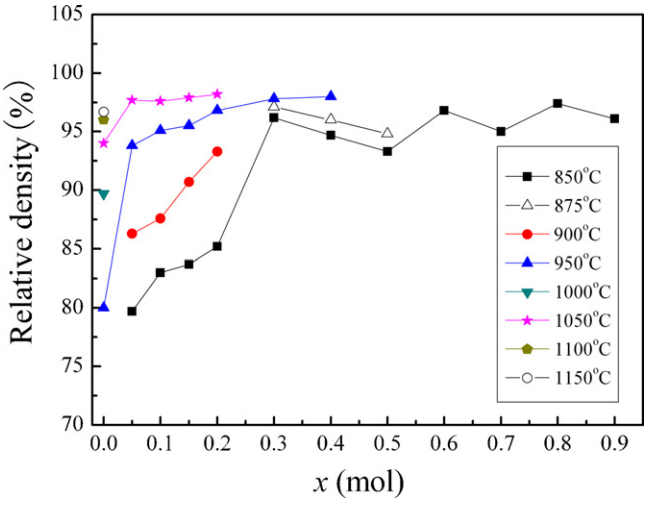

Fig. 4. Variation of relative density of $(1-x)Li_3NbO_4$–$xLiF$ ($0 < x \leq 0.9$) with x and sintering temperature.

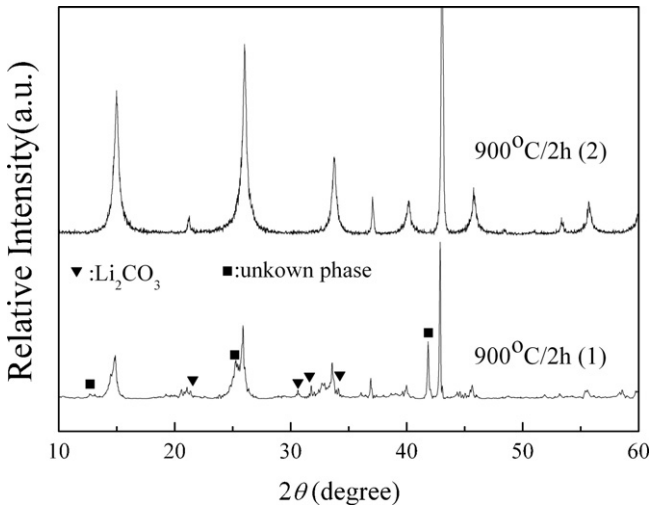

Fig. 5. Powder XRD patterns of Li_3NbO_4 synthesized by two different methods: Li_3NbO_4 was synthesized at 900 °C/2 h by conventional solid-state reaction process (pattern 1), and the initial mixtures were subjected to preliminary low-temperature calcining at 500 °C for 20 h and subsequent calcining at 900 °C for 2 h (pattern 2).

temperature for an intermetallic compound due to the resulted internal stress that raises the driving force for sintering.[30] Furthermore the mobilities of the ions, and hence the diffusion rate in disordered state is much larger than that in ordered state. Thus the decrease in sintering temperature with increasing LiF content could be mainly ascribed to the decrease in order–disorder phase transition temperature as shown in Fig. 1. On the other hand, weakening of oxygen bond strength with the increasing substitution of F^- for O^{2-} and the substitution of smaller F^- for O^{2-} would also facilitate the diffusion process and thus reduce the sintering temperature.

It is noted that the pure Li_3NbO_4 ($x = 0$) in this study densified at higher temperature (1150 °C/2 h, 96.7% TD), compared with that reported (~930 °C/2 h, 97% TD). Only 80% theoretical density could be obtained after at sintering at 950 °C/2 h in

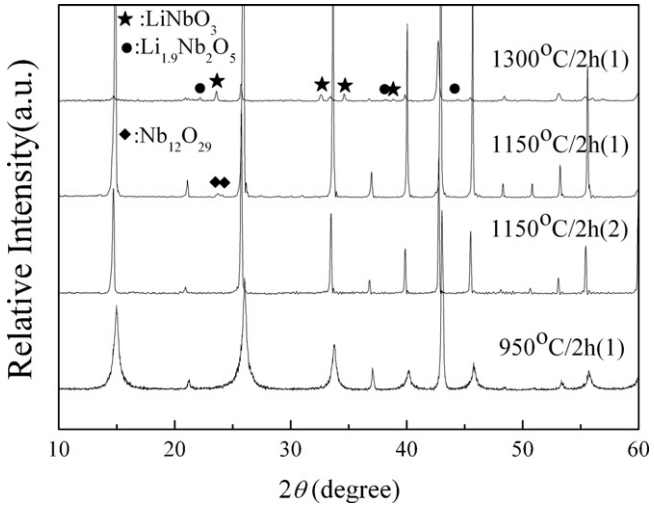

Fig. 6. Powder XRD patterns of Li_3NbO_4 sintered at different temperatures (patterns 1 and 2 correspond to the Li_3NbO_4 ceramics prepared without and with preliminary low-temperature calcining, respectively).

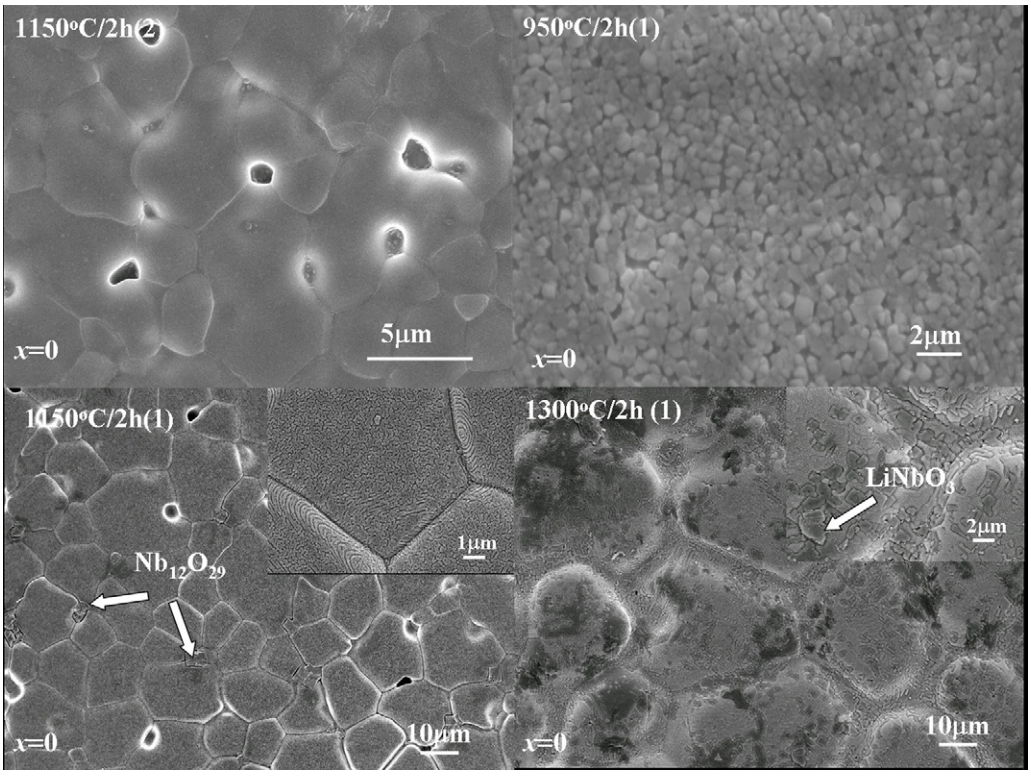

Fig. 7. SEM images of Li_3NbO_4 sintered at different temperatures (specimens 1 and 2 correspond to the Li_3NbO_4 ceramics prepared without and with preliminary low-temperature calcining, respectively).

this study, which is considerably lower than that reported by Zhou et al. The difference in sintering temperature may be related to the different synthesizing condition of Li_3NbO_4. Fig. 5 shows the powder XRD patterns of Li_3NbO_4 synthesized at 900 °C/2 h by conventional solid-state reaction process (pattern 1), and by preheating the initial mixtures at 500 °C for 20 h and subsequent calcining at 900 °C for 2 h (pattern 2). It demonstrates that single Li_3NbO_4 phase (I-43m) could be obtained at 900 °C/2 h with preliminary low-temperature calcining (pattern 2). In contrast, small amount of unreacted Li_2CO_3 and unknown intermediate compound(s) existed in addition to the Li_3NbO_4 phase after calcining at the same temperature without preliminary low-temperature calcining (pattern 1). The powder XRD patterns and its corresponding SEM images of the sintered specimens are shown in Fig. 6 and Fig. 7, respectively. For the Li_3NbO_4 ceramics prepared without preliminary low-temperature calcining (specimen 1), homogeneous dense ceramic with small grain size (less than 1 μm) could be obtained after sintering at 950 °C/2 h. No impurity phase was observed although remained unreacted phases presented in the synthesized powders. The SEM image of the above specimen sintered at 950 °C/2 h in this study is very similar to that in the study of Zhou et al. (900 °C/2 h).[24] However trace amount of $Nb_{12}O_{29}$ impurity phase was detected when sintered at 1150 °C/2 h. It is also noted that there is significant "surface porosity" within the grains (inset), which is due to the Li volatilization during the sintering process. With further increase in sintering temperature, impurity phases such as Li_3NbO_3 and $Li_{1.9}Nb_2O_5$ were observed due to the increasing volatilization of Li. In contrast, no impurity phase such as $Nb_{12}O_{29}$ was detected for the Li_3NbO_4 ceramics sintered at 1150 °C/2 h when lithium evaporation was suppressed by preliminary low-temperature calcining during its synthesizing process (specimen 2). It shows that the specimen 2 in this study densified at higher temperature (1150 °C/2 h, 96.7% TD), compared with the specimen 1 (950 °C/2 h) or the reported (~930 °C/2 h, 97% TD).[24] From a comparison of the results obtained in this study, it can be concluded that, the sintering temperature of pure Li_3NbO_4 powders was about 1150 °C/2 h, whereas, the remained small amount of unreacted Li_2CO_3 in the calcined powders reduced the sintering temperature of Li_3NbO_4 to about 950 °C/2 h. The remained unreacted Li_2CO_3 which melts at about 723 °C would improve the sintering of Li_3NbO_4 as reactive liquid phase. Although there is no XRD pattern of the Li_3NbO_4 synthesized at 800 °C/2 h in the study of Zhou et al., we believe that the improvement of sinterability for Li_3NbO_4 in the study of Zhou et al. could be mainly ascribed to the transient reactive liquid phase sintering from the unreacted Li_2CO_3 in the calcined powders, which is in agreement with that described by Ref. 31.

The SEM images of sintered specimens with different LiF content are shown in Fig. 8. The addition of LiF made Li_3NbO_4 ceramic densify at 850 °C/2 h when $x \geq 0.4$. Furthermore, the grain size varied greatly with composition and sintering temperature. The $x = 0.1$ (1050 °C/2 h), $x = 0.2$ (1050 °C/2 h) and $x = 0.4$ (850 °C/2 h) specimens showed much smaller grain size (less than 1 μm) than that of $x = 0.4$ (950 °C/2 h), $x = 0.6$ (850 °C/2 h) and $x = 0.8$ (850 °C/2 h) specimens (5–10 μm). The growth rate of the grain of average size is described as $dg/dt = M_b\gamma/g$,[32]

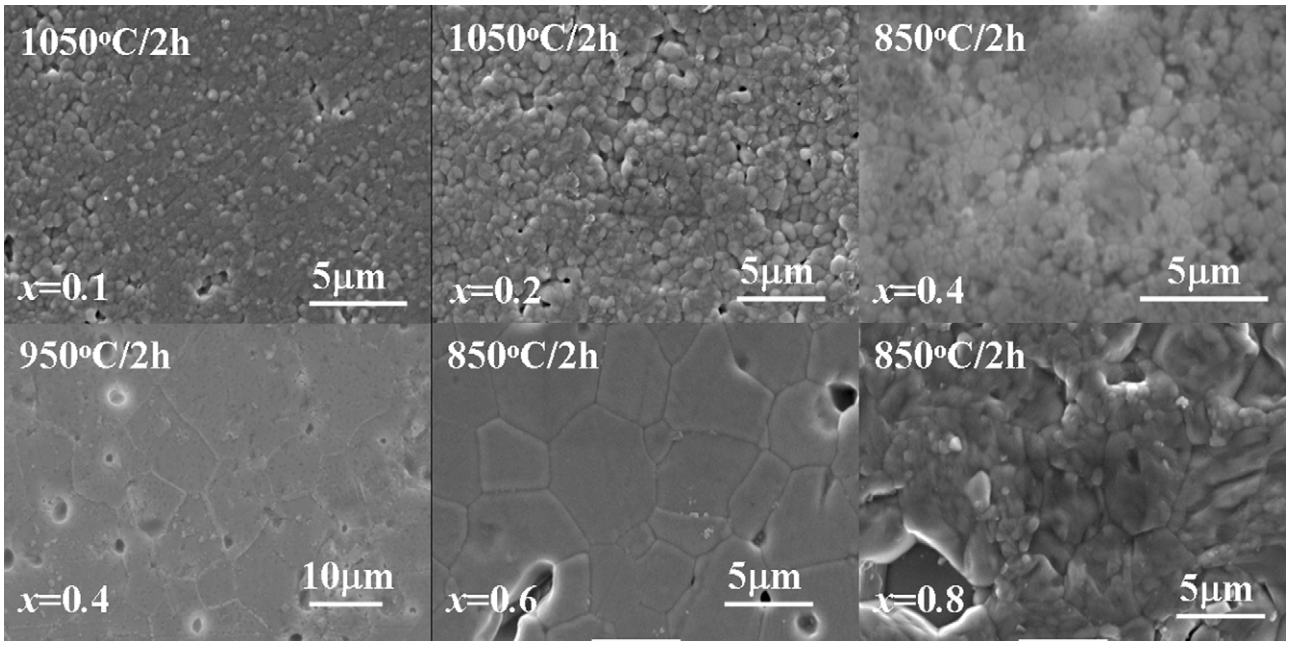

Fig. 8. SEM images of $(1-x)Li_3NbO_4$–$xLiF$ $(0<x\leq 0.9)$ sintered at different temperatures.

where g is the grain size, M_b is the grain boundary mobility and γ is the interfacial energy. The grain boundary mobility M_b is given by equation[32]: $M_b = (D_b\Omega)/\delta kT$, where Ω is the atomic volume, D_b is the boundary diffusion coefficient and δ is the boundary thickness. The interfacial energy γ should not change greatly. However the mobilities of ions, and hence the grain growth are expected to substantially increase when the phase changes from ordered into disordered state as discussed above. Therefore the sharp increase in grain size for $x=0.4$ composition as the sintering temperature increased from 850 °C/2 h to 950 °C/2 h could be ascribed to the corresponding phase transition from ordered body-centered cubic (I-43m) to long range disordered face-centered cubic phase (Fm-3m) as shown in Fig. 1. This also explained the larger grain size of $x=0.6$ (850 °C/2 h) and $x=0.8$ (850 °C/2 h) specimens both of which exhibited same disordered face-centered cubic phase (Fm-3m). Similar phenomenon was also observed in the sintering of Li_2TiO_3 ceramics.[31]

Fig. 9 shows the variation of dielectric properties as function of LiF content and sintering temperature. The dielectric permittivity increased with increasing sintering temperature for the fixed composition obviously due to the increase in relative density as shown in Fig. 4. However the optimized dielectric permittivity for each composition decreased with the increase of LiF content, which could be attributed to the comparative lower dielectric polarizabilities of Li^+ and F^- than that of Nb^{5+} and O^{2-}, respectively ($\alpha_D(Li^+)=1.2$ Å^3, $\alpha_D(Nb^{5+})=3.97$ Å^3, $\alpha_D(F^-)=1.62$ Å^3 and $\alpha_D(O^{2-})=2.01$ Å^3).[33] Fig. 10 shows the change of $Q\times f$ value with LiF content and sintering temperature. The $Q\times f$ value increased with increasing sintering temperature for each composition obviously due to the increase in relative density. The optimized $Q\times f$ value for each composition

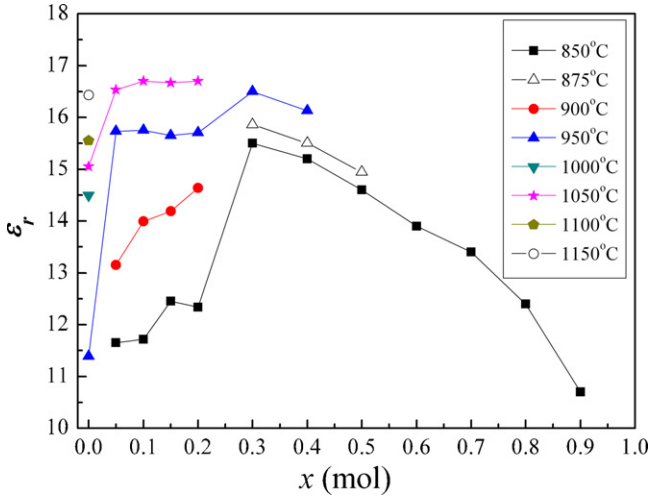

Fig. 9. Variation of relative permittivity of $(1-x)Li_3NbO_4$–$xLiF$ $(0<x\leq 0.9)$ ceramic with x and sintering temperature.

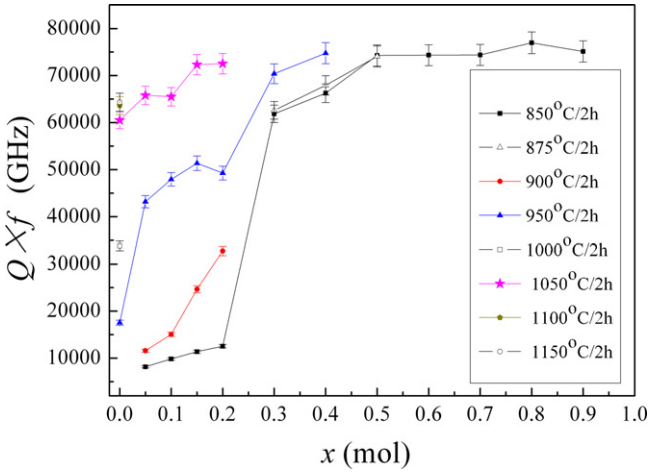

Fig. 10. Change of $Q\times f$ value of $(1-x)Li_3NbO_4$–$xLiF$ $(0<x\leq 0.9)$ ceramic with x and sintering temperature.

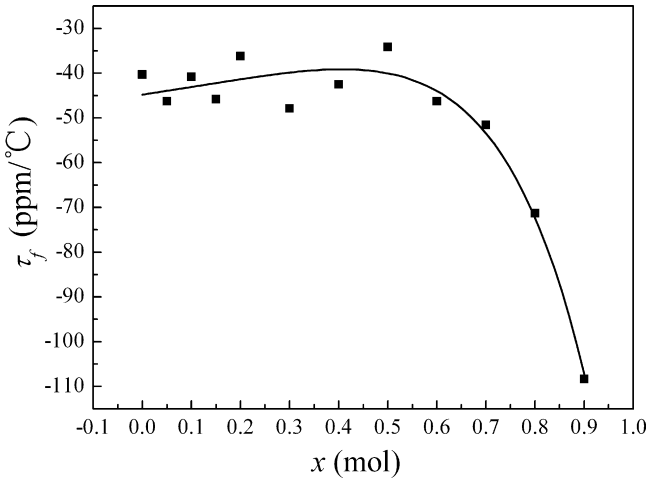

Fig. 11. Change of τ_f value of $(1-x)Li_3NbO_4$–$xLiF$ $(0<x\leq 0.9)$ ceramic with x.

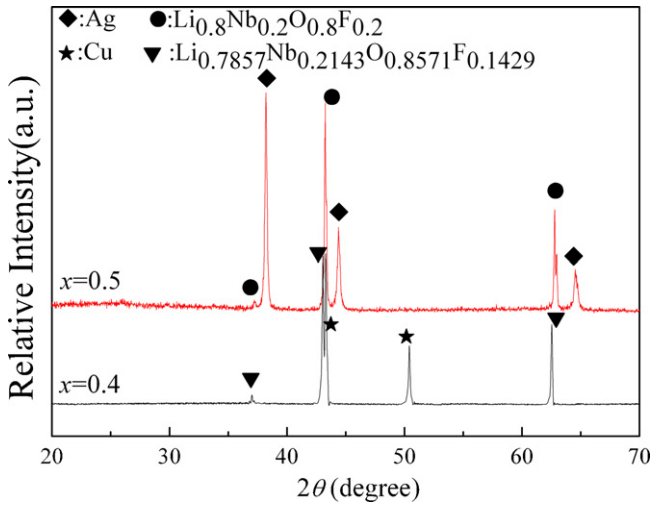

Fig. 12. XRD patterns of $x=0.4$ composition co-fired with Cu at 950 °C/2 h in N_2 atmosphere and $x=0.5$ composition co-fired with Ag at 850 °C/2 h in open air.

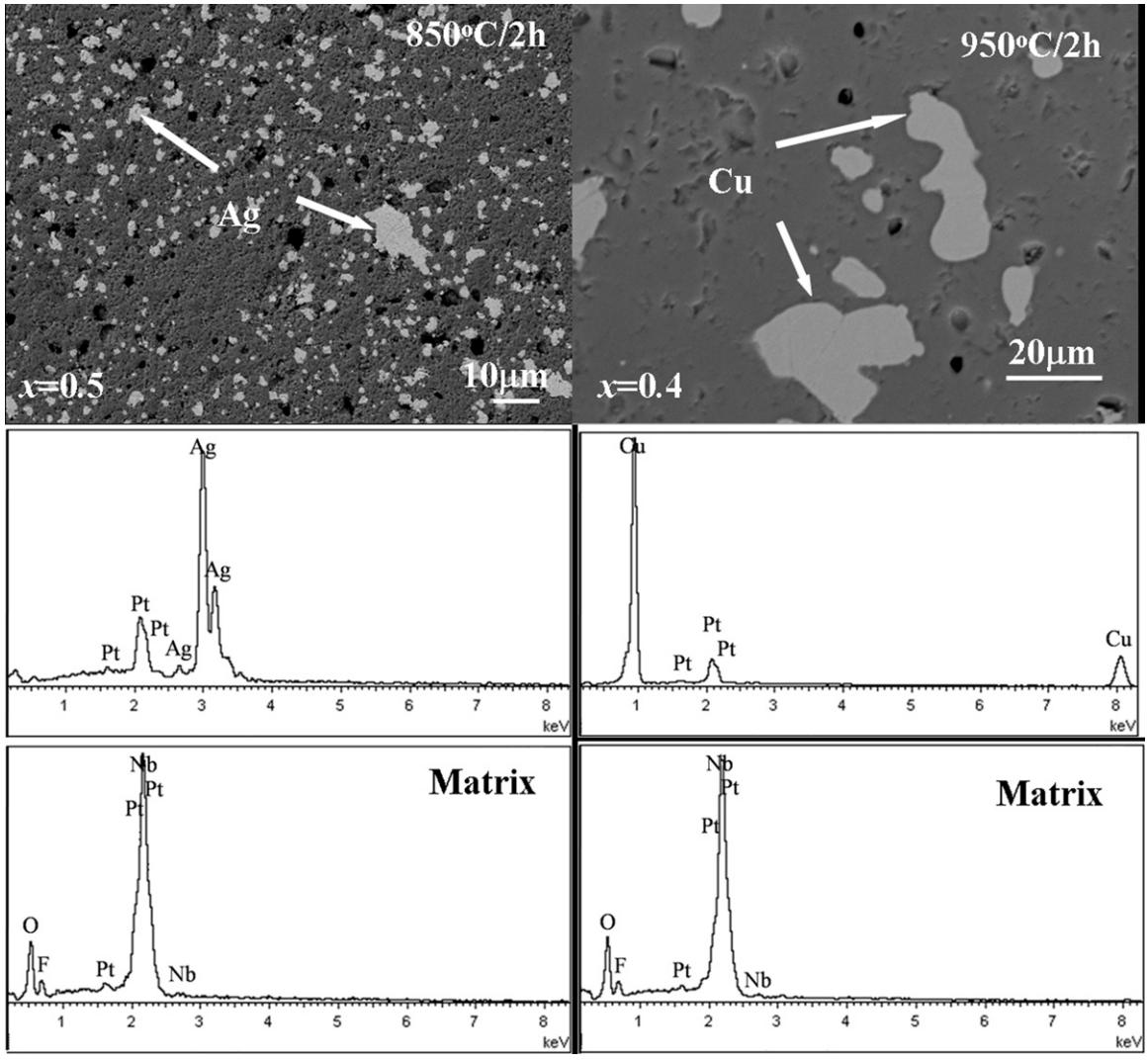

Fig. 13. Back scattered SEM images and corresponding EDS analysis of $x=0.4$ composition co-fired with Cu at 950 °C/2 h in N_2 atmosphere and $x=0.5$ composition co-fired with Ag at 850 °C/2 h in open air.

increased with the increase of LiF content and saturated at about 75,000 GHz when $x \geq 0.15$. Fig. 11 shows the variation of temperature coefficient of resonant frequency τ_f with LiF content. All specimens exhibited negative τ_f value. The absolute τ_f value decreased slightly with the increase of LiF content up to $x = 0.5$ and then increased greatly with the further increase of x.

The chemical compatibility with silver or copper was investigated by co-firing the mixed powders with pure silver (30 wt% Ag) or copper (30 wt% Cu) in ambient atmosphere at temperature of 850 °C for 2 h or N_2 atmosphere at 950 °C for 2 h, respectively. The powder XRD patterns of the $x = 0.5$ composition co-fired with Ag at 850 °C/2 h and $x = 0.4$ composition co-fired with Cu at 950 °C/2 h are shown in Fig. 12. The strong reflections from silver or copper could be identified easily. No impurity phase such as AgF or CuF_2 was detected within the experimental limitation, which seems to indicate that no chemical reaction has taken place between the matrix phase and Ag or Cu. The matrix phase of $x = 0.5$ composition co-fired with Ag at 850 °C/2 h in ambient atmosphere (unmuffled) exhibited face-centered cubic (Fm-3m) phase. In contrast the pure $x = 0.5$ composition sintered at 850 °C/2 h in N_2 atmosphere (muffled) showed body-centered cubic phase (I-43m). The phase transition may be caused by the increase of the F- or Li-loss (Fig. 2). The back scattered SEM images of the co-fired specimens are shown in Fig. 13. Two distinct phases-Ag or Cu and matrix could be easily identified. No visible reaction product is detected, which is agreement with the XRD results in Fig. 12.

4. Conclusions

Sintering behavior, microstructure and microwave dielectric properties of $(1-x)Li_3NbO_4$–$xLiF$ ($0 \leq x \leq 0.9$) ceramics have been studied in this paper. For the LiF-doped compositions, continuous solid solution formed in the whole compositional range. Phase transition from long range ordered body-centered cubic phase to long range disordered but short range ordered face-centered cubic phase occurred with the addition of LiF. Both the phase transition temperature and sintering temperature decreased with the increase of LiF content. The $x > 0.4$ compositions could be densified at 850 °C/2 h. The optimized $Q \times f$ value for each composition increased with the increase of LiF content and saturated at about 75,000 GHz when $x \geq 0.15$, whereas the optimized dielectric permittivity decreased with the increase of LiF content. All specimens exhibited negative τ_f value. The absolute τ_f value decreased slightly with the increase of LiF content up to $x = 0.5$ and then increased greatly with the further increase of x. The chemical compatibilities of $x = 0.4$ composition with copper (Cu) and $x = 0.5$ composition with silver (Ag) powders were also investigated. No chemical reaction has taken place between the matrix phase and Ag or Cu after sintering at 850 °C/2 h or 950 °C/2 h, respectively.

Acknowledgements

This work was supported by the National Science Foundation of China (NSFC) (project number: 50872081). The authors are also thankful to Mr. Lu Bo for recording XRD patterns (Rigaku D\max 2200, Tokyo, Japan) and Mr. Chu Yuliang for SEM (Apollo300, CamScan, UK).

References

1. Kagata H, Inoue T, Kato J. Low-fire bismuth-based dielectric ceramics for microwave use. *Jpn J Appl Phys* 1992;**31**:3152–5.
2. Kim HT, Nahm S, Byun JD. Low-Fire (Zn, Mg)TiO_3 microwave dielectrics. *J Am Ceram Soc* 1999;**82**(2):3476–80.
3. Kim D-W, Hong KS, Yoon CS, Kim CK. Low-temperature sintering and microwave dielectric properties of $Ba_5Nb_4O_{15}$–$BaNb_2O_6$ mixtures for LTCC applications. *J Eur Ceram Soc* 2003;**23**:2597–601.
4. Jantunen H, Rautiaho R, Uusimaki A, Leppavouri S. Compositions of $MgTiO_3$–$CaTiO_3$ ceramics with two borosilicate glasses for LTCC technology. *J Eur Ceram Soc* 2000;**20**:2331–6.
5. Jantunen H, Kangasvieri T, Vahakangas J, Leppavouri S. Design aspects of microwave components with LTCC technique. *J Eur Ceram Soc* 2003;**23**(14):2541–8.
6. Choi G, Stubbs MG, Park CS. A Kα and narrow band pass filter using LTCC technology. *IEEE Micro Wireless Comp Lett* 2003;**13**(9):388–9.
7. Valant M, Suvorov D. Glass-free low-temperature cofired ceramics: calcium germanates, silicates and tellurates. *J Eur Ceram Soc* 2004;**24**:1715–9.
8. Valant M, Suvorov D. Processing and dielectric properties of sillenite compounds $Bi_{12}MO_{20-\delta}$ (M = Si, Ge, Ti, Pb, Mn, $B_{1/2}P_{1/2}$). *J Am Ceram Soc* 2001;**84**(12):2900–4.
9. Bain JJ, Kim DW, Hong KS. Glass-free LTCC microwave dielectric ceramics. *Mater Res Bull* 2005;**40**:2120–9.
10. Subodh G, Sebastian MT. Glass-free $Zn_2Te_3O_8$ microwave ceramic for LTCC applications. *J Am Ceram Soc* 2007;**90**(7):2266–8.
11. Kwon DK, Lanagan MT, Shrout TR. Microwave dielectric properties and low-temperature cofiring of $BaTe_4O_9$ with aluminum metal electrode. *J Am Ceram Soc* 2005;**88**(12):3412–9.
12. Kwon DK, Lanagan MT, Shrout TR. Microwave dielectric properties of BaO–TeO_2 binary compounds. *Mater Lett* 2007;**61**(8–9):1827–31.
13. Udovic M, Valant M, Suvrov D. Dielectric characterization of ceramics from TiO_2–TeO_2 system. *J Eur Ceram Soc* 2001;**21**:1735–8.
14. Udovic M, Valant M, Suvrov D. Phase formation and dielectric characterization of Bi_2O_3–TeO_2 system prepared in oxygen atmosphere. *J Am Ceram Soc* 2004;**87**(4):591–7.
15. Kwon DK, Lanagan MT, Shrout TR. Synthesis of $BaTiTe_3O_9$ ceramics for LTCC application and its dielectric properties. *J Ceram Soc Jpn* 2005;**113**(3):216–9.
16. Zhou D, Randall CA, Pang LX, Wang H, Guo J, Zhang GQ, et al. Microwave dielectric properties of Li_2WO_4 ceramic with ultra-low sintering temperature. *J Am Ceram Soc* 2011;**94**(2):348–50.
17. Zhou D, Randall CA, Pang LX, Wang H, Wu XG, Guo J, et al. Microwave dielectric properties of $Li_2(M^{2+})_2Mo_3O_{12}$ and $Li_3(M^{3+})Mo_3O_{12}$ (M = Zn, Ca, Al, and In) lyonsite-related-type ceramics with ultra-low sintering temperatures. *J Am Ceram Soc* 2011;**94**(3):802–5.
18. Ohsahi M, Ogawa H, Kan A, Tanaka E. Microwave dielectric properties of low-temperature sintered $Li_3AlB_2O_6$ ceramic. *J Eur Ceram Soc* 2005;**25**:2877–81.
19. Li YZ, Bian JJ, Yuan LL. A new glass-free low-temperature fired microwave ceramic. *J Mater Sci* 2009;**44**:328–30.
20. Bian JJ, Kim DW, Hong KS. Microwave dielectric properties of $A_2P_2O_7$ (A = Ca, Sr, Ba, Zn, Mn, Mg). *Jpn J Appl Phys* 2004;**43**(6A):3521–5.
21. Bian JJ, Wu JY. Designing of glass-free LTCC microwave ceramic-$Ca_{1-x}(Li_{0.5}Nd_{0.5})_xWO_4$ by crystal chemistry. *J Am Ceram Soc* 2012;**95**(1):318–23.
22. Bian JJ, Wang L. Glass-free LTCC microwave ceramic-$(La_{0.5}Na_{0.5})_{1-x}(Li_{0.5}Nd_{0.5})_xWO_4$. *J Am Ceram Soc* 2011;**94**(10):3188–91.
23. Bian JJ, Liang Z, Wang L. Structural evolution and microwave dielectric properties of $Li_{(3-3x)}M_{4x}Nb_{(1-x)}O_4$ (M = Mg, Zn; $0 \leq x \leq 0.9$). *J Am Ceram Soc* 2011;**94**(5):447–53.
24. Zhou D, Wang H, Peng LX, Yao X, Wu XG. Microwave dielectric characterization of Li_3NbO_4 ceramic and its chemical compatibility with silver. *J Am Ceram Soc* 2008;**91**(12):4115–7.

25. Grenier JC, Bassi G. Structure refinement of Li_3NbO_4. *Bull Soc Fr Miner Crystallogr* 1965;**88**:345–6.
26. Ukei K, Suzuki H, Shishido T, Fukuda T. Li_3NbO_4. *Acta Crystallogr C* 1994;**50**:655–6.
27. Mather GC, Dussarrat C, Etourneau J, West AR. A review of cation-ordered rock salt superstructure oxides. *J Mater Chem* 2000;**10**:2219–30.
28. Castellanos M, West AR. Order–disorder phenomena in oxides with rock salt structure: the system Li_2TiO_3–MgO. *J Mater Sci* 1979;**14**:450–4.
29. Shannon RD. Revised effective ionic radii and systematic studies of interatomic distances in halides and chalcogenides. *Acta Crystallogr A* 1976;**32**:751–67.
30. Tournon J, Kuczynski GC. Diffusion coefficients from sintering of Al–Cu alloy wires. *Scripta Met* 1971;**5**:333–6.
31. Bian JJ, Dong YF. Sintering behavior, microstructure and microwave dielectric properties of $Li_{2+x}TiO_3$ ($0 \leq x \leq 0.2$). *Mater Sci Eng B* 2011;**176**:147–51.
32. Chang YM, Birnie DP, Kingery WD. *Physical ceramics – principles for ceramic science and engineering*. New York: John Wiley & Sons, Inc.; 1997. p. 375–376.
33. Shannon RD. Dielectric polarizabilities of ions in oxides and fluorides. *J Appl Phys* 1993;**73**(1):348–65.